

L_4, L_5 SOLAR SAIL TRANSFERS AND TRAJECTORY DESIGN: SOLAR OBSERVATIONS AND POTENTIAL EARTH TROJAN EXPLORATION

Rohan Sood* and Kathleen Howell†

The Sun-Earth triangular Lagrange point, L_5 , provides an ideal location to monitor the space weather. Furthermore, L_4, L_5 may harbor Earth Trojans and space dust that are of significant interest to the scientific community. No spacecraft has entered an orbit in the vicinity of Sun-Earth triangular points in part because of high propellant costs. By incorporating solar sail dynamics in the CR3BP, the concept of a mission to L_4, L_5 can be re-evaluated and the total ΔV can be reconsidered. A solar sail is employed to increase the energy of the spacecraft and deliver the spacecraft to an orbit about the artificial Lagrange point by leveraging solar radiation pressure and potentially without any insertion ΔV .

INTRODUCTION

Successfully harnessing the solar radiation pressure (SRP) from the Sun can potentially offer unique maneuvering capability to a spacecraft equipped with solar sails. The concept of solar sailing relies on photons from the Sun to propel the spacecraft through the space environment by providing the sail-based spacecraft with continuous acceleration. In 2015, the US-based Planetary Society launched and successfully unfurled its 32 m² LightSail. The sail-craft was able to demonstrate the capability to successfully deploy the sail. Success of JAXA's IKAROS mission, along with several small to mid-sized solar sail mission concepts, have renewed interest in solar sailing.^{1,2}

SCIENTIFIC INTEREST

With the launch of International Sun/Earth Explorer 3 (ISEE-3) in 1978, the near vicinity of the Sun-Earth L_1 libration point has been the preferred location for placing satellites to monitor space weather. However, as the satellite is positioned along the Sun-Earth line, observations of Coronal Mass Ejections (CMEs) heading directly towards the Earth are not feasible due to occultation. In addition, the observation of Co-rotating Interaction Regions (CIRs) from the vicinity of L_1 is not advantageous since the time between observations and the arrival at Earth is not sufficient to allow preventative measures to minimize the damage. Over the recent years, the Sun-Earth L_5 region has been investigated for an Earth-Affecting Solar Cause Observatory (EASCO).³ The triangular point, L_5 , supplies an ideal location for monitoring the space weather away from the Sun-Earth line and can aid in early detection of CMEs and CIRs. Early detection can offer 3-5 days advanced warnings of space weather that can potentially cause severe damage to telecommunications on Earth.

In addition to providing a unique angle to monitor the Sun and assess space weather, the equilateral Lagrange points, $L_{4,5}$, may harbor asteroids and space dust that are of significant interest to the scientific community. In 2010, NASA's Wide-field Infrared Survey Explorer (WISE) spacecraft identified the first Earth Trojan Asteroid (2010 TK₇) in the vicinity of L_4 .⁴ A near-Earth Asteroid, 2010 SO₁₆, is currently in the

*Ph.D. Candidate, School of Aeronautics and Astronautics, Purdue University, 701 West Stadium Avenue, West Lafayette, IN 47907-2045, USA. rsood@purdue.edu

†Hsu Lo Distinguished Professor of Aeronautics and Astronautics, School of Aeronautics and Astronautics, Purdue University, 701 West Stadium Avenue, West Lafayette, IN 47907-2045, USA. 765-494-5786, howell@purdue.edu

vicinity of Sun-Earth L_5 and is possibly a horseshoe companion of the Earth.⁵ The discoveries have opened a window for possible missions and scientific exploration of the bodies themselves as well as the region in the vicinity of the triangular Lagrange points in search of additional Earth Trojans at both L_4 and L_5 . The composition of Earth Trojan asteroids can potentially be similar to the rocks that formed the Earth about 4.6 billion years ago. Examination of such bodies - those from the time of the birth of the solar system - can shed new light on the composition of the Earth during its birth and early stages of development.

OBJECTIVES

The goal of this investigation is an exploration of the design space for trajectories from a parking orbit about Earth to the vicinity of artificial triangular Lagrange points using a solar sail. Prior to incorporating the sail dynamical model in the Circular Restricted Three-Body Problem (CR3BP), a set of solutions are derived based on the trajectory requirements. Initial solutions are computed that incorporate multiple ΔV s to depart the parking orbit around Earth, shift onto the manifold towards a desired destination and insert into an orbit in the vicinity of the equilateral Lagrange point, L_4 or L_5 . Initial investigation aims at better understanding the behavior of a sail-based spacecraft and leveraging the solar radiation pressure to deliver the spacecraft to its destination. The analysis addresses the goal of this investigation through the following objectives:

1. Explore the design space by computing a large set of L_1 and L_2 orbits and their manifolds.
2. Exploit orbits based on their energy and manifolds that reach the desired destination, i.e., vicinity of L_4 or L_5 .
3. Incorporate solar sails to maneuver the spacecraft and increase the energy level by leveraging SRP.
4. Investigate the departure ΔV from an Earth parking orbit.

By investigating the natural dynamics and flow that exists within the context of the CR3BP, a preliminary trajectory is designed to depart the vicinity of the Earth, shift onto a manifold towards the desired target and enter the orbit in the vicinity of $L_{4,5}$. The selection of a manifold is based on the target Lagrange point, i.e., L_4 or L_5 , energy level of the desired final orbit around the equilateral Lagrange point and the time of flight (TOF) to reach the vicinity of the target along the manifold. An initial departure ΔV is implemented to depart the parking orbit and leverage a stable/unstable manifold. Intermediate ΔV (s) can raise the energy level of the trajectory or serve as a trajectory corrective maneuver. Once the spacecraft reaches the vicinity of the target destination, a final ΔV may be necessary to insert into an orbit about the equilateral Lagrange point. The complete end-to-end trajectory acts as an initial guess for a corrections process that incorporates a solar sail force model into the circular restricted three-body problem (SS-CR3BP).

Incorporating the solar sail in the CR3BP potentially lowers the ΔV requirements by leveraging the solar radiation pressure. As a part of this effort, the solar sail is employed to increase the energy of the spacecraft in lieu of energy raising maneuvers and to deliver the spacecraft to an artificial triangular Lagrange point potentially without any insertion ΔV . Once the corrected final path is achieved, the trajectory is potentially optimized to lower the departure ΔV from the Earth parking orbit.

PREVIOUS CONTRIBUTIONS

Trajectory and mission design to Sun-Earth L_4, L_5

In recent years, trajectories to Sun-Earth equilateral Lagrange points have been the focus of a number of applications. With L_5 as an ideal location for early detection and observation of potentially hazardous space weather and the discovery of the first Earth Trojan Asteroid, 2010 TK7, in the vicinity of L_4 , the Sun-Earth triangular Lagrange points have gained interest as candidates for future space missions. Detailed analysis of an L_5 mission to observe the Sun and assess the space weather was completed by Lo, Llanos and Hintz.⁶ In 2011, Llanos, Miller and Hintz continued this work and provided navigational analysis for a mission to L_5 .⁷ Gopalswamy et al.⁸ proposed the Earth Affecting Solar Cause Observatory (EASCO) mission concept

that detailed the scientific issues and instruments necessary to monitor and understand the CMEs and CIRs. Further analysis from EASCO was carried out at the Mission Design Laboratory (MDL), NASA Goddard Space Flight Center and is aimed towards observing the solar maximum in the year 2025.³ The results of the MDL study determined that the EASCO mission concept is very achievable as a single observatory carrying 10 science instruments. The authors state that the L_5 point is the next logical location for obtaining solar observation of CMEs that direct solar energetic particles towards the Earth and cause geomagnetic storms. In the following year, Llanos, Miller and Hintz extended their work to incorporate trajectory design to both L_4 and L_5 in the Sun-Earth System.⁹ The goal was a strategy to study the Sun's magnetic field from a vantage point near L_5 and search for Earth Trojan Asteroids in the vicinity of L_4 and L_5 .

With the discovery of Earth Trojan 2010 TK7, the scientific community is intrigued with the idea of additional, smaller asteroids, and space dust in the vicinity of the Sun-Earth triangular Lagrange points. The possibility of investigating the bodies that may be of similar composition to the rocks that formed the Earth is also of interest. Dvorak et al. completed an extensive investigation on the orbit of 2010 TK7 to better understand the motion of bodies in the vicinity of triangular Lagrange points.¹⁰ Based on their analysis, the authors predict the existence of additional 'interesting objects' in the vicinity of the L_4 or L_5 equilibrium points. In 2013, Llanos et al. also studied powered heteroclinic and homoclinic connections between the Sun-Earth Lagrange points L_4 , L_5 and the quasi-satellite orbit about Earth.¹¹ Such a transfer trajectory can potentially be used to transfer sample material from the triangular points to the vicinity of the Earth. A team of scientists from NASA Johnson Space Center presented their work on a mission concept at the 46th Lunar and Planetary Science Conference, 2015 proposing an in-situ science and exploration mission to survey the L_4 and L_5 regions in the Sun-Earth system.¹²

Solar sails

Exploring the use of solar sails to move throughout the solar system is based on a dynamical concept for harnessing the energy carried by photons from the Sun in the form of momentum. Although serious planning to explore the solar system using solar sails has only gained momentum in last few decades, the concept of harnessing solar radiation pressure (SRP) was first studied in 1873 by James Clerk Maxwell.¹³ In 2010, the first spacecraft to demonstrate the use of solar radiation pressure as a source of propulsion in flight was launched by the Japanese Space Agency, JAXA. The solar sail spacecraft, Interplanetary Kite-craft Accelerated by Radiation Of the Sun (IKAROS), is a square sail 20 m in diameter and 7.5 μm thick created from polyimide film. IKAROS successfully demonstrated both a propulsive force of 1.12 mN and attitude control capabilities.¹⁴ Thus, IKAROS delivered a pathway for further development in the field of solar sail technology.

On May 20, 2015, the Planetary Society successfully launched LightSail-A, a precursor to LightSail-1, as a small technology demonstrator aboard an Atlas V rocket from Cape Canaveral Air Force Station, Florida. The spacecraft was able to successfully deploy its 5.6m x 5.6m solar sail on June 7, 2015 and the test flight was declared a success.¹⁵ LightSail-1 is currently scheduled for a launch in April 2016. Upon the successful testing of LightSail-1, LightSail-2 is planned for launch to further enhance the solar sail based control strategy. It is expected that LightSail-3 will follow with a proposed mission that incorporates an insertion into an orbit near the Sun-Earth Lagrangian point, L_1 . LightSail-3 will provide early detection and warning of geomagnetic storms capable of damaging power and communications systems on Earth.¹⁶ Thus, the recent success and rejuvenation of interest in harnessing the potential of a solar sail has accelerated the development of technology. The success of the IKAROS mission and demonstration by LightSail-A are a significant breakthrough and, thus, interest continues in further testing and validating solar sail technology.

Considerable efforts have investigated solar sail behavior in the vicinity of the artificial collinear Lagrange points, L_1 and L_2 . Baoying and McInnes designed new orbits associated with these points by incorporating solar sails in the dynamical model.¹⁷ Their work applied knowledge of accurate approximation of 'Halo' orbits around equilibrium points.¹⁸ McInnes and Simmons focused on Sun-centered halo-type trajectories above the ecliptic plane aided by solar sails.¹⁹ In 2012, Sood further explored the solar sail applications to widen the design space in the vicinity of artificially displaced L_1 Lagrange points. Samples of offset, hovering periodic orbits are demonstrated above displaced L_1 and three-dimensional transfers between halo orbits are

constructed to exhibit sailing capabilities.²⁰ Solar sails have also been proposed for highly non-Keplerian orbits high above the ecliptic plane since solar sails are capable of supplying a continuous propulsive force in the form of SRP from the Sun.²¹ Recent work in the Earth-Moon system aims at investigating the behavior in the vicinity of displaced collinear Lagrange points and producing solar sail periodic orbits in the CR3BP.^{22, 23} Design of solar sail trajectories with applications to continuous surveillance of the lunar south pole have also been proposed.^{1, 2} Research in both the Sun-Earth and Earth Moon system have primarily been focused around displaced collinear Lagrange point or in the form of hovering orbits close to the primaries.

No known results have so far exploited the capabilities of solar sails to reach triangular Lagrange points. In addition, no spacecraft has reached an orbit about L_4 or L_5 due to high propellant costs associated with transfer and insertion into an orbit about an equilateral Lagrange point.⁶ Thus, solar sails can potentially deliver a viable mission concept by harnessing SRP for transfer trajectories and insertion maneuvers around artificial L_4 or L_5 points. In addition to demonstrating the technology, trajectory design to triangular points can aid in monitoring the space weather and searching for Earth Trojans or sampling space dust.

BACKGROUND: CIRCULAR RESTRICTED THREE-BODY PROBLEM

The motion of an infinitesimal mass, P_3 , under the gravitational influence of the two larger primaries, P_1 and P_2 , is investigated by studying the classical Circular Restricted Three-Body Problem (CR3BP). Casting the problem within the context of the CR3BP offers the essential features of the motion with some mathematical advantages. A rotating frame, R , is defined to be consistent with the orbital motion of the primaries. The dextral, orthogonal set of unit vectors associated with the rotating frame is denoted as \hat{x} ; \hat{y} ; \hat{z} where \hat{x} is always directed from P_1 to P_2 . The position vectors corresponding to the locations of the three bodies, P_1 , P_2 and P_3 , relative to the barycenter, are defined as \vec{r}_1 , \vec{r}_2 and \vec{r}_3 whereas \vec{r}_{13} and \vec{r}_{23} define the position vector of P_3 relative to P_1 and P_2 , respectively, as represented in Figure 1. Characteristic quantities, i.e., mass, length,

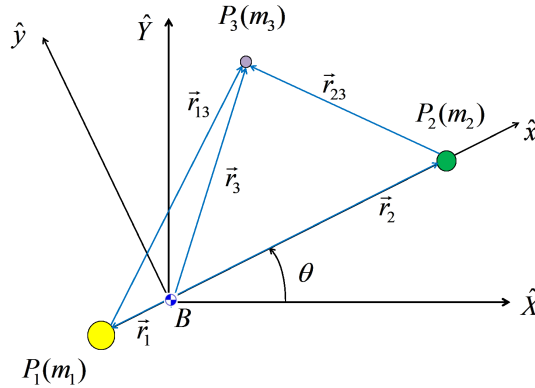


Figure 1: Geometrical Definitions in the Circular Restricted Three-Body Problem.

and time, are defined to generalize the governing differential equations through nondimensionalization such that

$$m^* = m_1 + m_2 \quad (1)$$

$$l^* = r_1 + r_2 \quad (2)$$

$$t^* = \sqrt{\frac{l^{*3}}{\tilde{G} m^*}} \quad (3)$$

where m_1 and m_2 are the masses of the two *primaries*, P_1 and P_2 , respectively, r_i is the distance between the system barycenter and the two primaries and \tilde{G} is the dimensional universal gravitational constant.

Nondimensional time and relative position vectors are then expressed in the form

$$\tau = \frac{t}{t^*} \quad (4)$$

$$\vec{\rho} = \frac{\vec{r}_3}{l^*} = x\hat{x} + y\hat{y} + z\hat{z} \quad (5)$$

$$\vec{d} = \frac{\vec{r}_{13}}{l^*} = (x + \mu)\hat{x} + y\hat{y} + z\hat{z} \quad (6)$$

$$\vec{r} = \frac{\vec{r}_{23}}{l^*} = (x - 1 + \mu)\hat{x} + y\hat{y} + z\hat{z} \quad (7)$$

where $\vec{\rho}$, \vec{d} , \vec{r} represent the nondimensional position vectors of P_3 relative to the barycenter, P_1 and P_2 , respectively.

Within the context of the CR3BP, five particular solutions exist in the rotating frame as depicted in Figure 2.²⁴ These equilibrium solutions, also termed the libration or Lagrangian points, were first recognized by Joseph-Louis Lagrange in 1772 while investigating the *three-body problem*.²⁵ L_1 , L_2 and L_3 are the

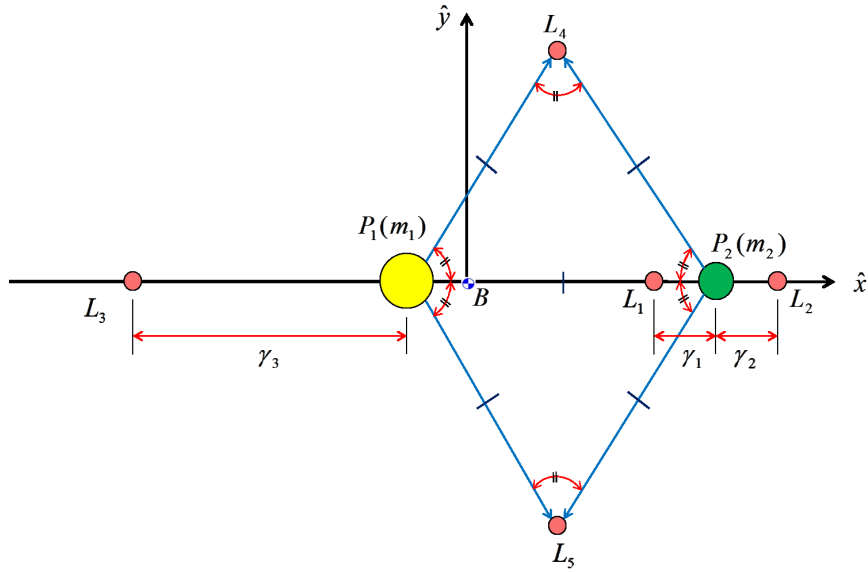


Figure 2: Lagrangian Points in the Circular Restricted Three-Body Problem.

collinear libration points, whereas, L_4 and L_5 are termed as ‘equilateral’ or ‘triangular’ Lagrange points since they form an equilateral triangle with the Sun and the Earth at the other two vertices. In a physical sense, the five particular solutions represent the locations where the combined influence from the two primaries, P_1 and P_2 , on the third body, P_3 , of negligible mass, are balanced within the context of the rotating frame.

Periodic orbits, invariant manifolds and Jacobi constant

Several fundamental periodic solutions exist in the vicinity of the equilibrium points that demonstrate their usefulness in trajectory and mission design. Families of planar and three-dimensional orbits have been investigated over the past few decades.²⁶ One type of planar periodic orbit is a simple symmetric orbit in the set that comprises the ‘Lyapunov’ family of orbits. A member of the L_1 Lyapunov family of orbits is illustrated in Figure 3(a). For visualization purpose, the Earth has been scaled to 20 times its actual size. In case of unstable periodic orbits, invariant manifold structures exist that grant passage into and away from the associated

orbit. Stable and unstable manifolds are computed by perturbing a state along the direction of stable or unstable eigenvector. Such perturbations result in a set of stable and unstable manifolds that exhibit asymptotic flow surface to and from the periodic orbit. A subset of unstable manifolds associated with the Sun-Earth

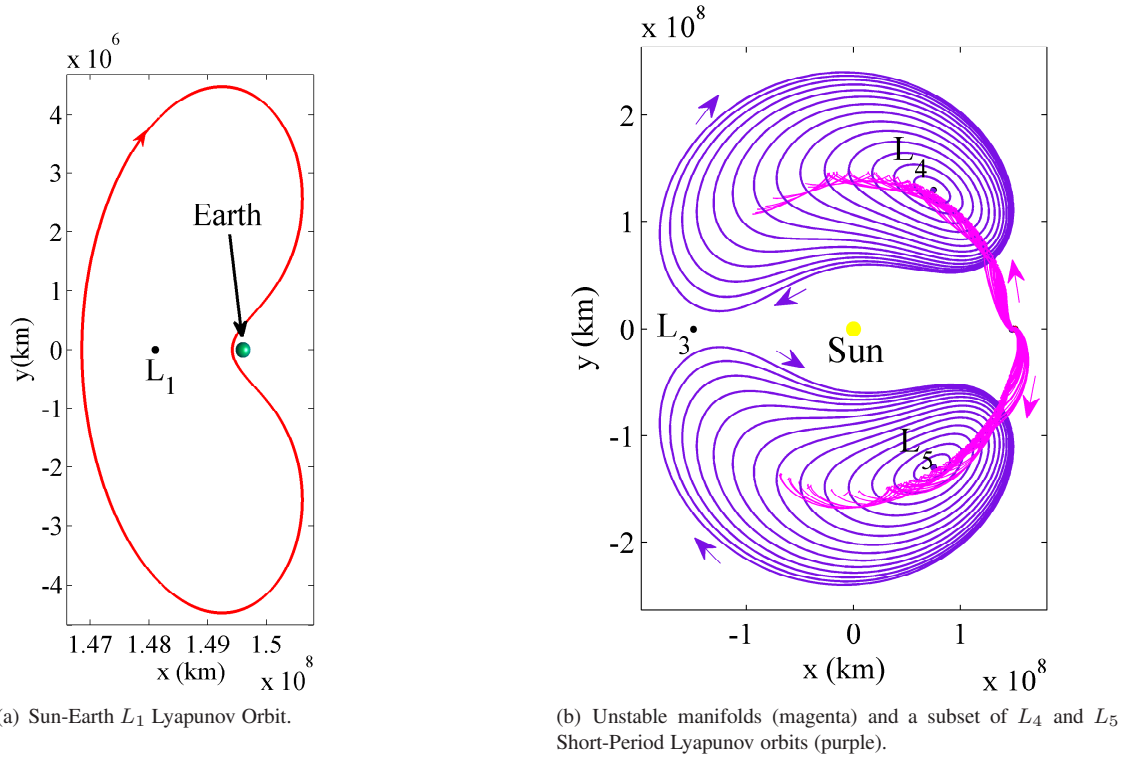


Figure 3: Periodic orbits and manifolds.

L_1 Lyapunov orbit in Figure 3(a) appears in Figure 3(b) as depicted in magenta. The unstable manifolds asymptotically depart the Lyapunov orbit and are propagated forward in time for 1800 days (approximately 5 years). The forward propagation demonstrates their flow approaching the two equilateral Lagrange points and the associated subset of short-period family of orbits about L_4 and L_5 are illustrated in purple. To construct low energy transfers, the invariant manifolds form an important tool in the computation and design of complex trajectories.

Within the context of the CR3BP, a unique known integral of motion, i.e., the Jacobi integral, may be defined. The Jacobi constant is a scalar and appears as an energy-like quantity for a particular orbit. Analysis employing the Jacobi constant is an effective approach to compute boundaries, orbits, trajectories and transfers. It also forms an important tool in maintaining accuracy in the numerical integration process. However, the addition of other external forces may eliminate the constant, yet it still provides a tool to gauge the changes in the energy-like quantity due to additional forces. The direction in which the Jacobi constant changes can potentially offer an insight into the pros and cons of additional force, thus, making it possible to exploit the force in delivering the spacecraft to its final destination and energy level.

SOLAR SAIL DYNAMICAL MODEL

The concept of harnessing the energy carried by photons from the Sun in the form of momentum extends the solar sail model into the CR3BP framework. In the development of a force model, a mathematical description of the direction of force relative to the sail orientation is a key kinematical relationship. The quantity of photons encountered by the solar sail is directly related to the sail orientation with respect to the direction of photon flow. Thus, the orientation of the sail governs the acceleration produced on the solar sail by the incident and the reflected photons. The momentum transfer from the incident and reflected

photons acting on a sail result in a net force that continuously accelerates the vehicle. The derivation of the acceleration due to solar radiation pressure is based on three critical assumptions. For preliminary analysis, it is assumed that the solar sail is ideal and flat with a perfectly reflecting surface, i.e., there is no absorption or refraction but only reflection due to the incident photons. Thus, all the photons experience perfectly elastic collisions and “bounce off” the surface of the solar sail. It is also assumed that the source of photons is the primary, P_1 , the Sun. The flow of incident photons is parallel to the Sun-sail line and the resultant force is parallel to the sail surface normal. Considering the assumptions, the solar sail acceleration is expressed as,

$$\vec{a}_{sail} = \epsilon \frac{2P_0}{\sigma} \cos^2 \alpha \hat{n} \quad (8)$$

where ϵ is the efficiency of the sail that typically ranges between 85% - 90% and P_0 is the solar radiation pressure at the distance of 1 AU from the source, i.e., the Sun. In Equation (8), the load factor, σ , is defined as the ratio of the total mass supported by the sail to the total surface area of the sail. Whereas, \hat{n} , is the unit direction vector in the direction parallel to the surface normal of the sail and is a function of the sail angles, α and γ . A new quantity is also defined as the solar sail characteristic acceleration, a^* . The characteristic acceleration is the acceleration at 1 AU and, for the particular orientation, such that the sail angle is equal to zero, i.e., $\alpha = 0^\circ$, or

$$a^* = \epsilon \frac{2 \times P_0}{\sigma} = \epsilon \frac{2 \times 4.56}{\sigma [\text{g/m}^2]} [\text{mm/s}^2] \quad (9)$$

The characteristic acceleration, a^* , serves as a reference value for comparison with general solar sail accelerations. Consistent with the definition of σ , a characteristic mass-to-area ratio, σ^* , is defined that produces a force equal and opposite to the force acting on the sail due to solar radiation pressure at 1 AU, i.e.,

$$\sigma^* = \epsilon \frac{2 \times P_0 r_{13}}{\tilde{G} m_1} \quad (10)$$

Recall that \tilde{G} is the dimensional universal gravitational constant, the quantity r_{13} is the dimensional scalar distance of the third body, i.e., the solar sail spacecraft, from the first primary, P_1 , the Sun and m_1 is the mass of the first primary, P_1 . The introduction of the sail lightness parameter, β , is appropriate as

$$\beta = \frac{\sigma^*}{\sigma} \quad (11)$$

The sail lightness parameter, also frequently denoted the sail loading parameter, is the ratio of the acceleration due to the solar radiation pressure to the classical solar gravitational acceleration.¹³ Thus, the solar sail acceleration expression in Equation (8), is set equal to one for efficiency, i.e., $\epsilon = 1$, and is rewritten as

$$\vec{a} = \beta \frac{\tilde{G} m_1}{r_{13}^2} \cos^2 \alpha \hat{n} \quad (12)$$

Now, rewriting Equation (12) in terms of nondimensional quantities

$$\ddot{\vec{r}}_{Sail} = \beta \frac{(1 - \mu)}{d^2} \cos^2 \alpha \hat{n} \quad (13)$$

where $\ddot{\vec{r}}_{Sail}$ is the nondimensional acceleration of the solar sail due to solar radiation pressure. Recall that d is the nondimensional distance of the solar sail from the Sun. The model for the nondimensional solar sail acceleration in Equation (13) is now easily included to augment the equations of motion in the classical CR3BP. Thus, a mathematical model that incorporates the solar sail dynamics in the CR3BP can be expressed in a condensed form of the equations of motion for a spacecraft equipped with solar sail and are written as

$$\ddot{x} = 2\dot{y} + \Omega_x^* + a_{Sail-x} \quad (14)$$

$$\ddot{y} = -2\dot{x} + \Omega_y^* + a_{Sail-y} \quad (15)$$

$$\ddot{z} = \Omega_z^* + a_{Sail-z} \quad (16)$$

where Ω_i^* are the partials of the pseudo-potential, and a_{Sail-x} , a_{Sail-y} , and a_{Sail-z} are the components of the nondimensional solar sail acceleration expressed in the rotating frame. The dynamical model represented in Equations (14) - (16) is nonlinear and coupled, thus, no closed-form solution exists.

PRELIMINARY RESULTS: SOLAR SAILING

Spacecraft trajectory design in the Circular Restricted Three Body Problem (CR3BP)

Investigating the design space that meets the mission and science requirements constitutes an integral part of the trajectory design process. Prior to incorporating the solar sail in the trajectory design process, a good initial guess is desirable. The process requires exploring the design space, i.e., the solution space that exists in the vicinity of the libration points. Each periodic orbit about the libration point has a Jacobi constant, the only integral of motion known to exist in the CR3BP. The manifolds associated with the libration point orbits provide natural flow to and from the orbit. The design strategy takes into account the following variables: (1) the Jacobi constant of the initial and final orbit, (2) the unstable manifold associated with the initial departure orbit, (3) the departure altitude relative to the Earth, (4) the insertion location along the final arrival orbit, and (5) the number of revolutions of the final orbit. In this section, intuitive search strategy is outlined by exploring the available design space. Flow away from the parent orbit, passing the vicinity of the Earth and departing towards the final destination are investigated. A baseline discontinuous trajectory is formulated as an initial guess for differential corrections algorithm.

Selection criteria – design space: The trajectory design process begins with the selection of a departure orbit based on the Jacobi value of the final desired orbit. However, this is not a required step but aids in exploiting possible low cost transfer options that may exist as the two orbits are of similar energy level. Jacobi values corresponding to a subset of L_1 , L_2 Lyapunov family and L_5 short period orbits are apparent in Figure 4(a). Visual analysis of Figure 4(a) conveys that, in general, the L_5 short period orbits (green) are

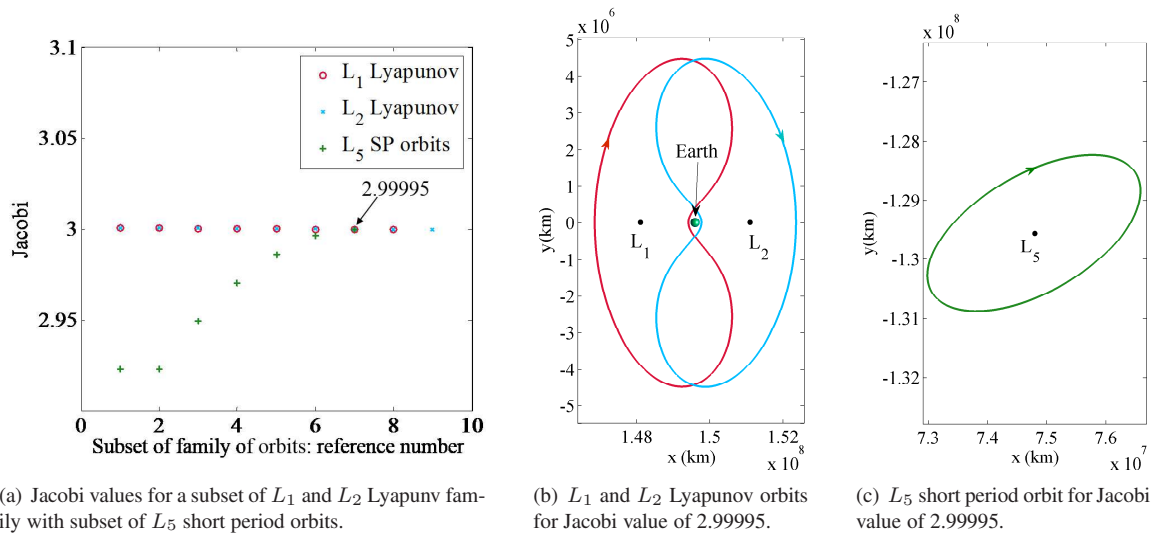


Figure 4: Jacobi analysis and periodic orbits.

of higher energy (lower Jacobi value) compared to the subset of L_1 and L_2 Lyapunov family of orbits (red and blue, respectively). For preliminary design analysis, a final orbit in the vicinity of L_5 is selected such that the Jacobi constant of the short period orbit is similar to that of the L_1 and L_2 Lyapunov orbits. Thus, orbits corresponding to a Jacobi value of 2.99995 are selected. In Figure 4(b), L_1 and L_2 Lyapunov orbits are depicted relative to the Earth in red and blue, respectively. Though it may visually appear, the two orbits are not mirror images (equal size) of each other. L_5 short period orbit for the same Jacobi value of 2.99995 is illustrated in Figure 4(c). Note that the size of the L_5 short period is two orders of magnitude greater than that of the L_1 and L_2 Lyapunv orbits, though the period of all three orbits is close to 1 year.

Trajectory design options: Continuing the design process, dynamical properties of manifolds are exploited. The Jacobi value associated with the manifolds remains conserved and possesses the same value as that of the parent orbit within the rotating frame. Employing manifolds to locate transfer option opens a window

to depart from a parking orbit onto a manifold of either L_1 or L_2 Lyapunov orbit and reach the vicinity of L_4 and L_5 to lower the mission cost. For each triangular Lagrange point, four possible transfer options are briefly described that may vary based on the time of flight, ΔV requirements or the overall scientific goal of the mission. Transfer options to L_4

- L_1 unstable manifold to L_4 : spacecraft departs from Earth parking orbit along L_1 unstable manifold to arrive in the vicinity of final destination orbit about L_4 .
- L_1 stable manifold to L_1 unstable manifold to L_4 : spacecraft departs from Earth parking orbit along L_1 stable manifold towards parent orbit. The spacecraft may get into an orbit about L_1 to carry out scientific experiments before departing along the unstable manifold towards its final destination orbit about L_4 .
- L_2 unstable manifold to L_4 : spacecraft leaves the parking orbit around the Earth along the unstable manifold associated with the L_2 orbit for final destination orbit about L_4 .
- L_2 stable manifold to L_2 unstable manifold to L_4 : spacecraft departs the Earth parking orbit along L_2 stable manifold towards parent orbit. Similar to option two, the spacecraft may get into an orbit about L_2 to carry out scientific experiments before departing along the unstable manifold towards its final destination orbit about L_4 .

Similarly, exploiting the Sun-Earth L_1 and L_2 Lyapunov orbit manifolds, trajectory design options to the vicinity of second triangular Lagrange point, L_5 , are listed below. Transfer options to L_5

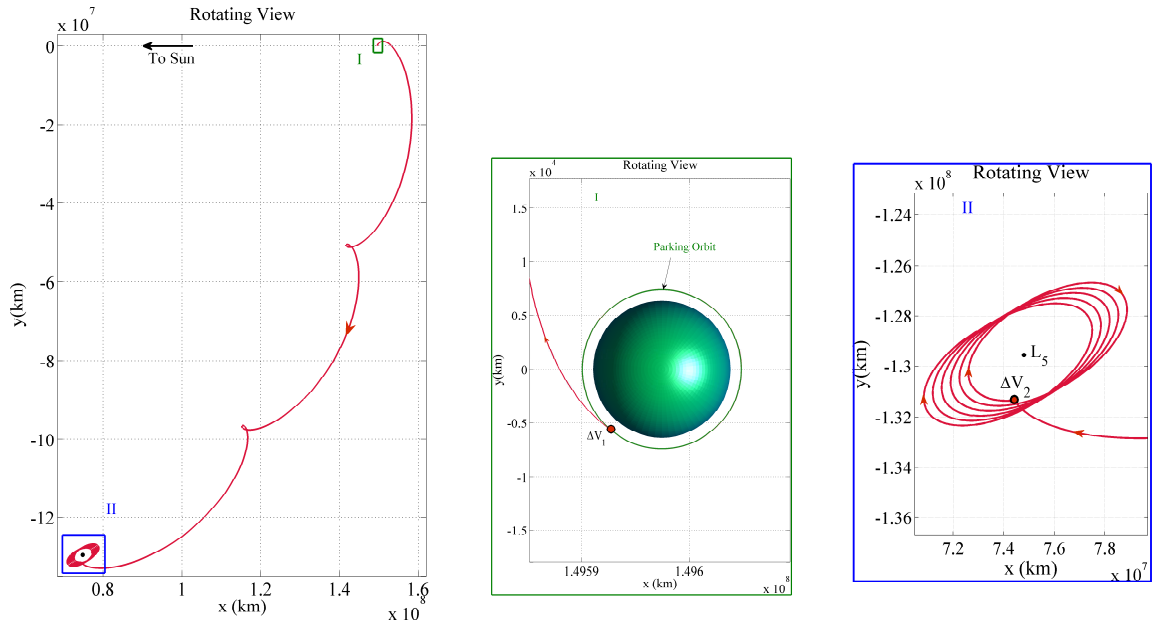
- L_1 unstable manifold to L_5 : spacecraft departs from Earth parking orbit along L_1 unstable manifold to arrive in the vicinity of final destination orbit about L_5 .
- L_1 stable manifold to L_1 unstable manifold to L_5 : spacecraft departs from Earth parking orbit along L_1 stable manifold towards parent orbit. The spacecraft may get into an orbit about L_1 to carry out scientific experiments before departing along the unstable manifold towards its final destination orbit about L_5 .
- L_2 unstable manifold to L_5 : spacecraft leaves the parking orbit around the Earth along the unstable manifold associated with the L_2 orbit for final destination orbit about L_5 .
- L_2 stable manifold to L_2 unstable manifold to L_5 : spacecraft departs the Earth parking orbit along L_2 stable manifold towards parent orbit. The possibility exists to station the spacecraft in an orbit about L_2 to carry out scientific experiments before departing along the unstable manifold towards its final destination orbit about L_5 .

Differential correction and baseline trajectory: Exploiting the fundamental solutions (libration point orbits, stable/unstable manifolds) of the CR3BP, a baseline trajectory is constructed that acts as an initial guess in the trajectory design process. The initial guess, a discontinuous trajectory, encompasses the following arcs in the design process: (1) parking orbit about Earth, (2) stable/unstable or a combination of the two manifolds, (3) arrival at the destination orbit, and (4) insertion into final orbit about the equilateral Lagrange point.

As an example of the trajectory design process, consider the L_1 Lyapunov orbit and the L_5 short period orbit depicted in Figures 4(b) and 4(c), respectively. Recall, the two orbits are of the same Jacobi value of 2.99995. Thus, the unstable manifold that originates from the L_1 Lyapunov orbit and is propagated until it reaches the vicinity of the destination L_5 short period orbit is of the same energy level as the two orbits. Initially, the spacecraft is stationed in a parking orbit around the Earth. The selection of departure altitude plays an important role in the trajectory design process. As the goal of the work is to incorporate solar sail in the final model, it is desirable to depart from an altitude higher than 800 km. At the altitude of 800 km, the solar radiation pressure and the atmospheric drag are equal. Thus, for the sail to operate efficiently, the recommended altitude is between 800 to 1000 km.²⁷ In this formulation, a circular Earth parking orbit with

an altitude of 1000 km is selected. At the departure location, ΔV is performed to transfer the spacecraft from the parking orbit onto the L_1 orbit's unstable manifold. The manifold is propagated until it reaches the vicinity of destination short period orbit about L_5 . It is possible to perform energy increasing maneuvers along the path. In the example presented with no sail, a final ΔV is permitted to get into the final orbit. Thus, the initial guess to the corrections scheme allows performing two ΔV s to deliver the spacecraft from the Earth parking orbit into an orbit about the L_5 triangular Lagrange point.

Baseline trajectory design is accomplished through the application of a differential corrections scheme to a two-point boundary value problem (2PBVP). Algorithm based on generalized Newton's Method is employed that involve constraints and free variables. A multiple shooting scheme is applied to reduce the effect of local sensitivities by distributing them among the individual arcs, increasing the accuracy and incorporating relative ease with which constraints can be placed along the trajectory and free variables can be selected. Distribution of sensitivities may also allow the convergence of solutions that may not appear using only one arc. The application of multiple shooting scheme enables placement of constraints at multiple locations along the path rather than just at the end points. Constraints are applied to fix the departure altitude at 1000 km where application of ΔV is allowed in the corrections scheme. Upon arrival in the vicinity of the destination orbit, the second ΔV is performed to deliver the spacecraft from the transfer arc to the final destination about L_5 . The constraint for the final trajectory is applied to maintain the spacecraft in the vicinity of L_5 for a duration of 5 years. The resultant corrected trajectory is depicted in Figure 5(a). Position continuity is enforced along the entire path and velocity continuity is additionally enforced along the path except at the two maneuver locations. Figures 5(b) and 5(c) illustrate close-up views of the two boxes marked I and II,



(a) Transfer trajectory from the vicinity of an Earth orbit to the vicinity of L_5 in the Sun-Earth system.

(b) Departure trajectory and ΔV_1 maneuver from Earth parking orbit.

(c) Arrival trajectory and ΔV_2 maneuver into vicinity of L_5 .

Figure 5: Corrected trajectory with two ΔV maneuvers.

respectively, in Figure 5(a). The trajectory appearing in Figure 5(b) corresponds to a departure from 1000 km parking orbit around the Earth. The location of departure maneuver, ΔV_1 , of 3.041 km/s is marked with a red dot. After the application of the instantaneous maneuver, the spacecraft transfers onto the manifold arc associated with an L_1 Lyapunov orbit towards its final destination in the vicinity of L_5 as depicted in Figure 5(c). Upon arrival, an insertion maneuver of 559 m/s is performed at the location marked by ΔV_2 . Thus, the total ΔV required for the transfer trajectory is $\Delta V_{total} = 3.6$ km/s. The total time of flight (TOF) for the transfer from the Earth parking orbit to arrival in the vicinity of L_5 is 2.879 years (approximately 1036 days).

Solar sail trajectory design to the vicinity of L_4, L_5

Preliminary design of trajectories in the SS-CR3BP is typically based on a differential corrections scheme. A numerical corrections approach from the CR3BP is extended to incorporate the solar sail angles. The inclusion of the effects of photons on the acceleration of a solar sail based spacecraft increases the complexity associated with the system model. For trajectory design, a two-point boundary value problem can be solved using a differential corrections scheme and implementing solar sail angles as additional design parameters. The corrections scheme is formulated to iteratively modify the initial states based on the linear estimated information available from the state transition matrix (STM).

Sail based differential correction: The inclusion of sail angles offers additional options for formulation of the shooting scheme. A number of shooting schemes incorporating solar sail angles have been formulated and presented in previous work.²⁰ In this work, variable-time multiple shooting scheme is developed in which the trajectory is decomposed into a set of arcs, identified in terms of n discrete points, denoted as ‘patch-points’, allowing more flexibility in the corrections process. The overall objective of a multiple shooting differential corrections algorithm is a complete trajectory that is continuous in position and velocity. To achieve such continuity, orientation angles associated with the solar sail are iteratively updated to result in a final converged path. Note that the orientation angles remain fixed relative to the rotating frame over the integration time between two patch points. Allowing the integration time, τ_i , to vary along any segment, further extends the capabilities of using sail angles in the multiple shooting scheme, thus, resulting in the formulation of variable-time multiple shooting algorithm. The updated design variable vector, \vec{X} now includes additional variables, τ_i . Thus, \vec{X} is a $(9n - 1) \times 1$ vector since there are $n - 1$ integration times corresponding to $n - 1$ arcs between n patch points, i.e.,

$$\vec{X} = \begin{Bmatrix} \vec{X}_1(8 \times 1) \\ \vdots \\ \vec{X}_n(8 \times 1) \\ \tau_1 \\ \vdots \\ \tau_{n-1} \end{Bmatrix} \quad (17)$$

Note that \vec{X}_i is an eight-dimensional vector comprised of three position states, three velocity states, and two orientation angles. The constraint vector, $\vec{F}(\vec{X})$ is defined to maintain continuity in both position and velocity states.

$$\vec{F}(\vec{X}) = \begin{Bmatrix} \vec{X}_1(\tau_{f_1})[1 : 6] - \vec{X}_2(\tau_{0_2})[1 : 6] \\ \vec{X}_2(\tau_{f_2})[1 : 6] - \vec{X}_3(\tau_{0_3})[1 : 6] \\ \vdots \\ \vec{X}_{n-1}(\tau_{f_{n-1}})[1 : 6] - \vec{X}_n(\tau_{0_n})[1 : 6] \\ ||\vec{r}(\tau_{0_1})|| - (\frac{1000km}{l^*}) \end{Bmatrix} \quad (18)$$

Continuity is maintained only for the six position and velocity states between each arc as denoted by $[1 : 6]$. The sail angles are free to differ between two arcs to achieve position and velocity continuity between two segments. Recall, \vec{r} represent the nondimensional position vectors of P_3 relative to P_2 . Final constraint in $\vec{F}(\vec{X})$ involves the altitude of the parking orbit and ensures that the departure altitude of 1000 km above the surface of the Earth is enforced during the corrections process. Thus, the dimensions of the constraint vector are $(6(n - 1) + 1) \times 1$ for $n - 1$ arcs between n patch points and the additional altitude constraint.

Incorporating sail angles in the multiple shooting algorithm results in modified Jacobian matrix. Many terms within the $D\vec{F}(\vec{X})$ matrix are recognized as the terms of the modified STM the $\phi_i(\tau_{f_i}, \tau_{0_i})$. Supplementing the two orientation angles as design variables, the STM, $\phi_i(\tau_{f_i}, \tau_{0_i})$ is a 6×8 dimensional matrix. Inclusion of integration time along each segment as additional design variables and the altitude as an addi-

tional constraints, the $D\vec{F}(\vec{X})$ matrix of dimensions $(6(n-1)+1) \times (9n-1)$ is written in the form

$$D\vec{F}(\vec{X}) = \begin{bmatrix} \phi_1(\tau_{f_1}, \tau_{0_1}) & -H & 0 & 0 & \dots & 0 & \dot{\vec{X}}_1[1:6,1] \\ 0 & \phi_2(\tau_{f_2}, \tau_{0_2}) & -H & 0 & \dots & 0 & \dot{\vec{X}}_2[1:6,1] \\ \vdots & \ddots & \ddots & \ddots & \ddots & \vdots & \vdots \\ 0 & 0 & 0 & 0 & \phi_{n-1}(\tau_{f_{n-1}}, \tau_{0_{n-1}}) & -H & \dot{\vec{X}}_{n-1}[1:6,1] \\ \frac{\partial ||\vec{r}(\tau_{0_1})||}{\partial \vec{p}}[1,1:3] & 0 & \dots & \dots & \dots & 0 & \end{bmatrix} \quad (19)$$

where H is a 6×8 rectangular diagonal matrix with diagonal entries equal to one. $\dot{\vec{X}}_i[1:6,1]$ represents the time derivatives corresponding to the position and velocity states at the end point along the reference segment, $\vec{X}_i[1:6,1]$. The last row of $D\vec{F}(\vec{X})$ matrix holds the partials for the altitude constraint in the columns corresponding to the initial position state.

Lightness parameter selection: The sail lightness parameter, also frequently denoted as the sail loading parameter, is the ratio of the acceleration due to the solar radiation pressure to the classical solar gravitational acceleration used to parameterize the solar sail efficiency. Even though the value for the lightness parameter within the range 0.03 - 0.3 reflects the current technology capabilities, recent IKAROS mission had β value of approximately 0.001.²⁸ McDonald and McInnes conducted a recent review of solar sail technology and discussed potential short-, mid-, and long-term solar sail missions with applicable lightness parameter.²⁹ The lightness number for the short-term, GeoStorm mission is calculated as $\beta \approx 0.02$ and $\beta \approx 0.1$ for the mid-term Solar Polar Orbiter. As for the long-term mission goal, $\beta \approx 0.3 - 0.6$ is calculated for the Interstellar Heliopause Probe. Heiligers and McInnes calculated the β in the range of 0.0388 to 0.0455 for the Sunjammer mission.³⁰ With solar sail technology still in the developmental stages, analyzing the behavior of solar sails with low sail lightness parameters may be more useful in near term mission design and analysis.

Solar sail transfer family to L_5 : Trajectory design incorporating a solar sail begins with the selection of a baseline solution computed in subsubsection and plotted in Figure 5 as an initial guess to the design process. The goal of a solar sail is to lower the ΔV requirement for the mission by performing a single departure ΔV from Earth parking orbit, accelerating the sail using SRP from the Sun, entering and maintaining the path in the vicinity of destination orbit using the sail itself. Note that, no insertion ΔV is performed to arrive at the final orbit around L_5 . Prior to building a family of transfer trajectories, an initial value of sail parameter, β value of 0.042 is selected for preliminary trajectory design. Employing the sail-based differential corrector and continuation in β , a subset of transfer trajectories are constructed for β in the range of 0.005 - 0.06 as depicted in Figure 6(a). The range for β is selected keeping in mind the near-term capabilities in the field of solar sail technology. Two trajectories for β values of 0.005 and 0.06 are marked. The blue arrow indicated the direction of increasing β . During the continuation scheme, steps are taken in β in intervals of 0.001 but for clarity, only a subset of transfer trajectories are plotted in Figure 6. A zoomed-in view for the transfer trajectories departing Earth parking orbit appears in Figure 6(b). Once again, the departure altitude is constrained to be at 1000 km above the surface of the Earth. The red dots mark the location of $\Delta V_{departure}$ for each trajectory departing from the Earth parking orbit for a specific value of β . Note that only the initial altitude is constrained and not the initial departure position vector relative to Earth, hence, the departure location is allowed to freely change during the corrections process as is evident from Figure 6(b).

Recall the definition of sail lightness parameter as the ratio of Solar Radiation pressure (SRP) acceleration to the gravitational acceleration, thus, providing a qualitative measure for the solar sail efficiency. As a result of varying the sail parameter, β for the transfer trajectory, each trajectory is capable of generating variable SRP with a specific upper bound. The amount of SRP acceleration generated governs the architecture of the trajectory and duration of time it takes for the trajectory to arrive at the vicinity of L_5 . In Figure 7(a), arrival for the subset of transfer trajectories appear for the family illustrated in Figure 6(a). The dotted-blue

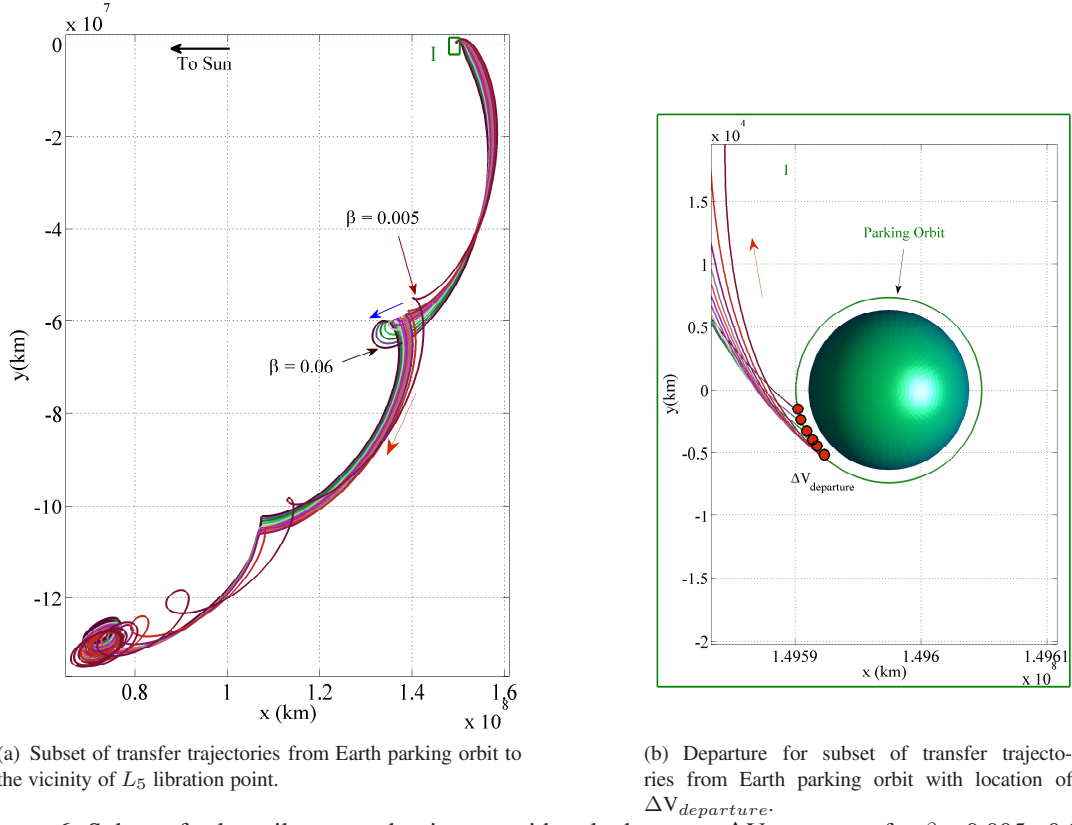
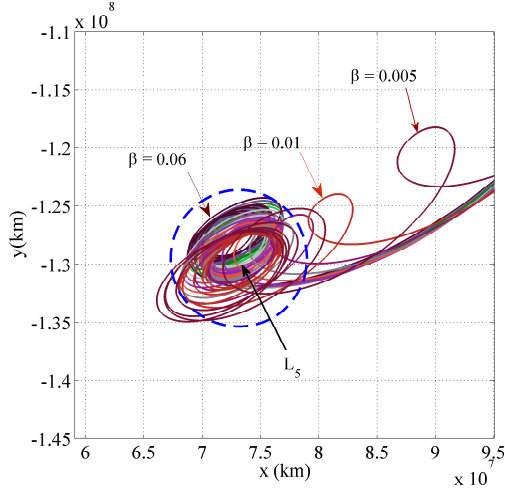


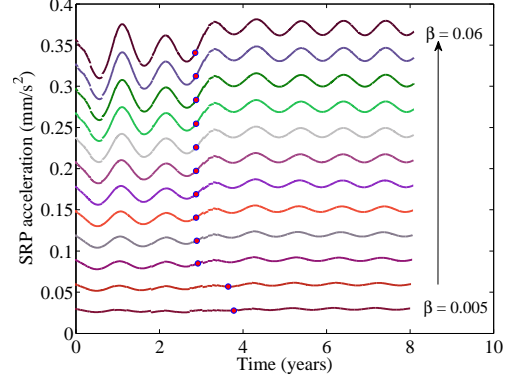
Figure 6: Subset of solar sail corrected trajectory with only departure ΔV maneuver for $\beta = 0.005 - 0.06$.

circle marks the location of arrival in the vicinity of the L_5 Lagrangian point. The radius of the circle is ≈ 0.04 AU based on the amplitude of an L_5 short period orbit with Jacobi value equivalent to 2.99995 that was incorporated to find the initial transfer trajectory in the no-sail CR3BP. Three trajectories with their β values are marked to demonstrate how the flow varies as the sail parameter, β changes. Trajectories with lower β values (0.005 and 0.01) form additional ‘cusps’ prior to entering the dotted-blue circle that marks the arrival when compared to relatively higher β values, i.e. 0.06. The overall behavior of the trajectory, as it arrives the Lagrangian point, varies with the change in sail parameter. It is evident that, for the subset of transfer trajectories, higher values of β result in trajectories that are closer to the given initial guess. The higher the value of sail parameter β , the more SRP acceleration the sail-craft is capable of generating as apparent from Figure 7(b). As the time increases, the sail-craft with higher β values is able generate enough acceleration to maintain the spacecraft in the vicinity of L_5 much more efficiently when compared to trajectories with lower β values. As the SRP acceleration varies with the β value, the time of flight (TOF) it takes for each trajectory to enter the blue circle also changes. The magenta dots in Figure 7(b) marks the location for a specific transfer trajectory as it reaches the dotted-blue circle. As the β value decreases, the TOF increases relatively slowly as can be seen for the β values ranging from 0.06 - 0.015. Conversely, for sail parameter $\beta = 0.005$ and 0.01, the TOF increases by 9-12 months which is also evident from the formation of additional cusps seen in Figure 7(a). Upon arrival, the spacecraft remains in the vicinity of L_5 for at least 4-5 years to carry out assigned scientific mission. Of course, the duration of time spend can be altered based on the mission requirements.

Within the context of the CR3BP, Lagrange points are the equilibrium locations where the net gravitational forces of the two primaries completely offset the centripetal force in the rotating frame. Physically, such existing conditions imply that both the velocity and acceleration are zero relative to the rotating frame. With the addition of the solar sail to the force model of the CR3BP, new equilibrium solutions emerge in the form of artificial Lagrange points.¹⁹ Thus, for the transfer trajectories depicted in Figure 6(a), new artificial Lagrange points, L_5' are evaluated for β ranging from 0.005 - 0.06 and depicted in Figure 8. With the addition of



(a) Subset of solar sail corrected trajectory arrivals at L_5 for different β values. Blue dotted-circle marks the arrival of a transfer trajectory within the vicinity of L_5 .



(b) Variation in Solar Radiation Pressure (SRP) acceleration over time for transfer trajectories ranging from $\beta = 0.005$ - 0.06.

Figure 7: Subset of sail trajectories as they arrive in the vicinity of L_5 and the corresponding SRP over time.

SRP acceleration the equilibrium points shift towards the Sun as the value of sail parameter, β increases. The artificial Lagrange points depicted are for case corresponding to sail angle, $\alpha = 0$, i.e., the sail is head-on relative to the Sun-sail direction. For $\beta = 0$, the solar sail model generates a special case for the conditions corresponding to the classical CR3BP. Tradition L_5 , that is associated with the classical CR3BP, is marked by a black dot. With each transfer trajectory, the value of β is stepped up by 0.005 that results in an equivalent shift of $\approx 200,000$ km. For sail parameter, $\beta = 0.06$, the total displacement of the artificial equilibrium point relative to traditional L_5 is ≈ 3 million km (0.02 AU). Thus, a spacecraft in the vicinity of displaced Lagrange point, L_5' can monitor the solar weather relatively closer than a spacecraft around the traditional Lagrange point, L_5 . Early detection of potentially hazardous solar weather can provide advanced warnings to take appropriate measures to minimize the damage at Earth. The single known integral of motion, denoted as the Jacobi constant, exists in the classical CR3BP. In Solar Sail Circular Restricted Three Body Problem (SS-CR3BP), the Jacobi value is no longer a constant. However, investigating the change in the Jacobi value helps in analyzing the effects of SRP acceleration on the energy level of the spacecraft as apparent in Figure 9(a). In addition to the β values in the range 0.005 - 0.06 being investigated in this section, lower values of $\beta = 0.002$ and 0.003 are added to help gain insight into the general trend for the change in Jacobi value over time as the photons continue to bombard the sail-craft. As an example, for $\beta = 0.003$ (light-blue), Figure 9(a) shows that the sail-craft is able to lower Jacobi (increase energy) over the duration of the flight. Quantitative decrease in Jacobi for a specific β value will be discussed in the following section. It is evident from the general trend that for higher values of sail parameter, β , the variation in Jacobi is higher. Hence, with higher β values, the energy of the trajectory can be significantly increased using solar sails. Although the spacecraft builds-up momentum as a result of harnessing SRP from the Sun, the initial boost is provided to help the spacecraft get on a path (manifold) towards the destination. The initial boost is delivered in the form of $\Delta V_{departure}$ that is required to depart from 1000 km Earth parking orbit as illustrated in Figure 9(b). Note that the $\Delta V_{departure}$ for a particular value of β depicted in this figure is non-optimal. Recall, each transfer trajectory is built

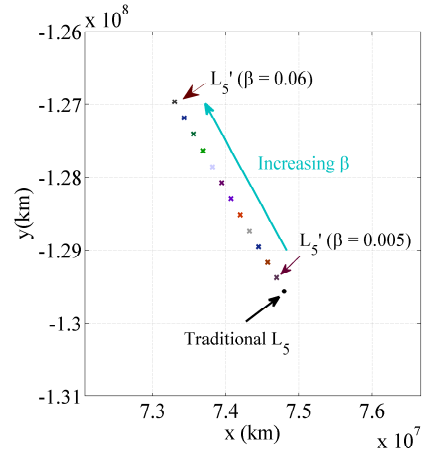


Figure 8: Artificial Lagrange points, L_5' for $\beta = 0.005 - 0.06$ relative to traditional Lagrange point L_5 .

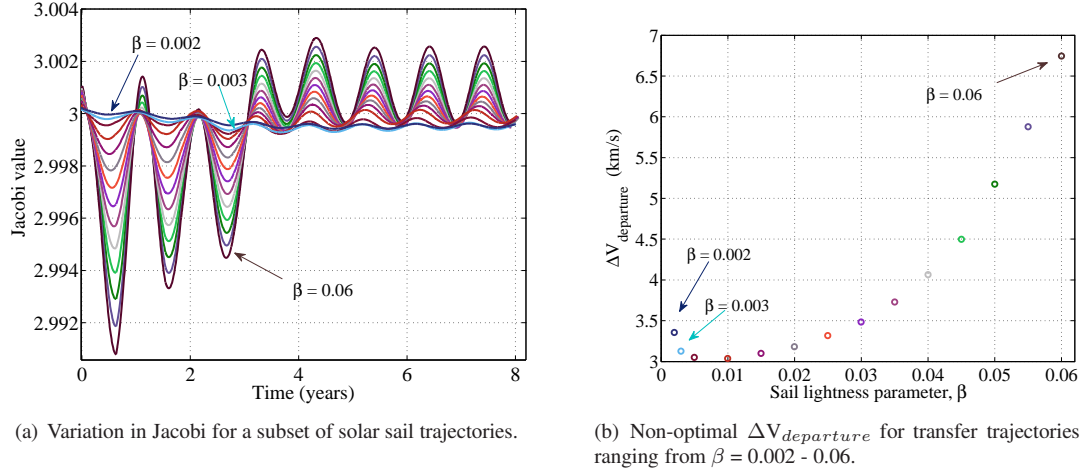


Figure 9: Jacobi analysis and non-optimal $\Delta V_{departure}$.

on continuation in sail parameter, β . Further analysis is carried out to optimize the solution to lower the $\Delta V_{departure}$ requirements.

Solar sail trajectory analysis: To understand the behavior of sail-based spacecraft and gain both qualitative and quantitative insight, a single transfer trajectory is investigated. Recall that the family was built for lower values of sail parameters for which continuation was carried out in steps of $\delta\beta = 0.001$. Taking into consideration the advancement in solar sail technology, $\beta = 0.022$ is selected for further analysis. The transfer trajectory for the sail parameter value of 0.022 is extracted and plotted as illustrated in Figure 10. A baseline trajectory from CR3BP is used as an initial guess for the sail-based dynamical model. The overall transfer trajectory is depicted in Figure 10(a). The red transfer trajectory is the initial guess derived in the CR3BP,

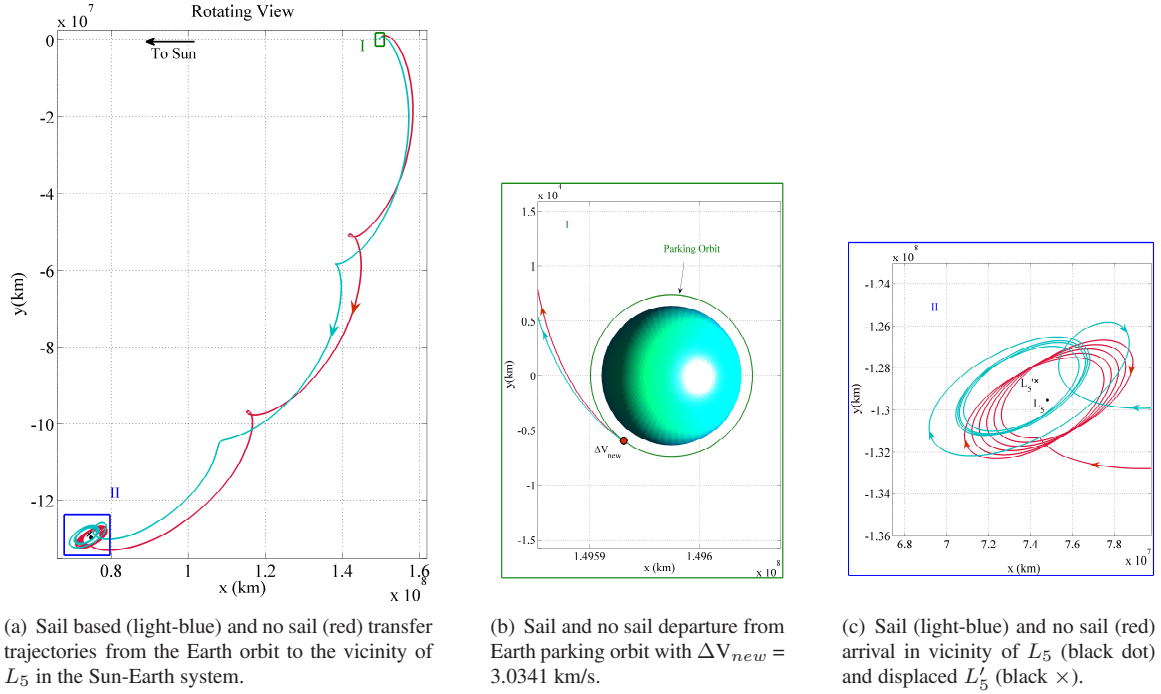


Figure 10: Solar sail corrected trajectory with one ΔV maneuver for $\beta = 0.022$.

whereas, the sail-based corrected trajectory for $\beta = 0.022$ is depicted in light-blue. Earth departure from a 1000 km parking orbit is illustrated in Figure 10(b). As a result of including solar sail in the dynamical model, only one ΔV is performed for the transfer trajectory. The ΔV is delivered to insert from the Earth parking orbit onto a trajectory towards the final destination using solar sails. The location of impulsive departure ΔV is marked by ΔV_{new} and is equivalent to 3.0341 km/s. The arrival transfer trajectories for both the CR3BP and SS-CR3BP are plotted in Figure 10(c). The velocity discontinuity in the red transfer trajectory (CR3BP) is the location where ΔV_2 was performed to deliver the spacecraft in the vicinity of L_5 for the baseline case (with no sail). As a result of incorporating solar sail, no insertion ΔV is required as evident from the light-blue transfer trajectory. Also note the displacement of artificial Lagrange point, L_5' relative to traditional Lagrange point, L_5 . The net displacement is ≈ 1.05 million km (0.007 AU) towards the larger primary, P_1 , i.e., the Sun as a result of SRP acceleration acting on the sail-craft.

In the CR3BP, the Jacobi value represents the constant of motion within the rotating frame. The Jacobi value for a trajectory is conserved when no additional forces, i.e., ΔV s, SRP are taken into consideration. ΔV maneuver results in a change in Jacobi constant. Jacobi values for two cases, no sail and sail-based ($\beta = 0.022$) trajectories are apparent in Figure 11. The red line represents the case with no sail in the dynamical model. The first jump of 0.0608 in Jacobi value (at Time = 0 years) is representative of departure ΔV performed to leave the Earth parking orbit and is equivalent to $\Delta V_1 = 3.041$ km/s. Note the discontinuity added at the top of $y - axis$ for Jacobi value of the departure orbit. The second jump (at Time = 2.9 years) marks the location where ΔV_2 of 559 m/s is performed to further raise the energy (lower Jacobi by 1.896×10^{-4}) of the trajectory to insert the spacecraft in an orbit about L_5 Lagrange point. Thus, in no sail case, the required $\Delta V_{total} = 3.6$ km/s to deliver the spacecraft from a 1000 km parking orbit to the vicinity of L_5 . The case exploiting solar sail technology with β of 0.022 is depicted in light-blue. Only one ΔV is performed that is delivered at the initial time to depart the Earth parking orbit marked as ΔV_{new} equivalent to 3.034 km/s. Note, no secondary ΔV is performed to insert the spacecraft in an orbit about L_5 , instead, the solar sail leverages SRP to increase the energy of the spacecraft and arrive in a final trajectory about displaced L_5' . The TOF for the sail-based spacecraft is 2.92 years (magenta dot) and exceeds the case with no sail by only ≈ 16 days. In this scenario, incorporating solar sails in the dynamical model (SS-CR3BP) assisted in accomplishing trajectory design to an artificial Sun-Earth L_5 by harnessing the SRP.

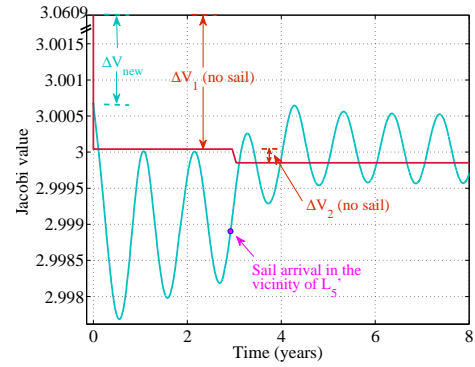


Figure 11: Jacobi analysis of transfer trajectories with no sail (red) and with sail (light-blue) for $\beta = 0.002$.

The magnitude and the direction of the SRP acceleration generated is governed by the orientation of the sail relative to the Sun-sail line. Within the context of SS-CR3BP, two sail angles are defined as clock angle, α and pitch angle, γ to orient the sail in the rotating frame. For the initial analysis of solar sail, motion in the $x - y$ plane is investigated that is governed by the clock angle α . Recall, the algorithm presented incorporates turn and hold strategy in which the sail maintains a constant orientation along an arc between two successive path points relative to the Sun-sail line in the rotating frame. However, from a mission perspective, it is important to analyze the sail angles from an inertial observer as the sail is continuously rotating along each arc relative to the Sun. Thus, α is expressed in the inertial frame as angle ψ relative to the inertial $\hat{X} - axis$ depicted in Figure 12(a) undergoing continuous rotation as viewed by an inertial observer. The values for ψ range between $\pm 180^\circ$ in the inertial frame relative to $\hat{X} - axis$. The rate of change in orientation (slope) of the sail in the inertial frame is $\approx 1^\circ/\text{day}$. The discontinuity in the figure is not physical but an artifact of the definition and bounds of sail angle ψ in the inertial frame. To determine the practicality of the trajectory, it is vital to consider hardware constraints that govern sail pointing accuracy, turn-rate and gimbal properties, i.e., maximum gimbal torque, maximum gimbal angle, and maximum gimbal rate. The absolute values for the change in sail orientation angle, $|\Delta\psi|$, required for the trajectory are illustrated in Figure 12(b) for the duration of 8 years. For a $40 \times 40 \text{ m}^2$ sail, Wie established a maximum roll-control torque of $\pm 1.34 \times 10^{-3} \text{ N}\cdot\text{m}$ and the maximum pitch and yaw-control torques of $\pm 1.45 \times 10^{-3} \text{ N}\cdot\text{m}$ that are capable of

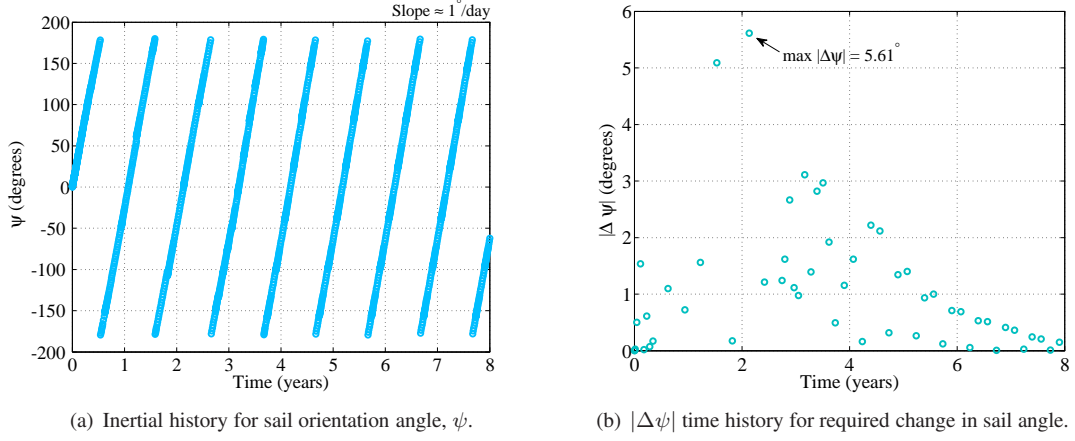


Figure 12: Solar sail orientation angle analysis in the inertial frame.

producing maximum angular accelerations of $\pm 13.0 \times 10^{-6} \text{ deg/s}^2$ and $\pm 28.1 \times 10^{-6} \text{ deg/s}^2$, respectively.³¹ The maximum turn rate for a three-axis stabilized spacecraft was set at 0.02 deg/s . Thus, the time to reorient the solar sail by a maximum value of $|\Delta\psi| = 5.61^\circ$ is ≈ 4 minutes 40 seconds. In the Sun-Earth system, the reorientation time span is more acceptable as compared to the Earth-Moon system.

Optimization

By incorporating solar sail dynamics in the CR3BP, corrections scheme is utilized to build a family of transfers from the Earth parking orbit to the vicinity of L_5 for various sail parameter, β . Utilization of design tools, such as periodic orbits, invariant manifolds, the Jacobi value analyses, can potentially give low-cost transfers, but they do not guarantee an optimal solution. However, solutions achieved from studying these inherent properties of the CR3BP regime can assist in formulating a good initial guess for the optimization problem. The objective is to deliver the spacecraft from an Earth parking orbit to the sail-based trajectory towards the final destination, L_5 . The initial ΔV maneuver (and the only ΔV) forms the primary performance measure that directly impacts the fuel requirements for the mission. Thus, minimization of the departure ΔV maneuver is the main focus for the optimization process based on the transfer trajectory design requirements.

The general architecture for the optimization process encompasses finding a set of design variables, \vec{X} , that can minimize or maximize the objective (cost) function, $f(\vec{X})$ and is subject to equality constraints, $\vec{F}(\vec{X}) = 0$ or inequality constraints, $\vec{F}(\vec{X}) \leq 0$. Analysis for a fuel optimal transfer between Earth parking orbit and the final destination in the vicinity of displaced Lagrange point, L_5 , is formulated as a minimization problem of a constrained nonlinear multivariable function. Identifying the design variables from Equation 17 with the objective of minimizing $\Delta V_{\text{departure}}$ subject to equality constraint of Equation 18, $\vec{F}(\vec{X}) \leq 0$, the optimization problem is stated as

$$\text{minimize} \quad f(\vec{X}) = \left\| \Delta \vec{V}_{\text{departure}} \right\|^2 = (V_{x_1} - V_{x_c})^2 + (V_{y_1} - V_{y_c})^2 + (V_{z_1} - V_{z_c})^2 \quad (20)$$

$$\text{subject to} \quad \vec{F}(\vec{X}) = \begin{Bmatrix} \vec{X}_1(\tau_{f_1})[1:6] - \vec{X}_2(\tau_{0_2})[1:6] \\ \vec{X}_2(\tau_{f_2})[1:6] - \vec{X}_3(\tau_{0_3})[1:6] \\ \vdots \\ \vec{X}_{n-1}(\tau_{f_{n-1}})[1:6] - \vec{X}_n(\tau_{0_n})[1:6] \\ \left\| \vec{r}(\tau_{0_1}) \right\| - \left(\frac{1000 \text{ km}}{l^*} \right) \end{Bmatrix} = \vec{0} \quad (21)$$

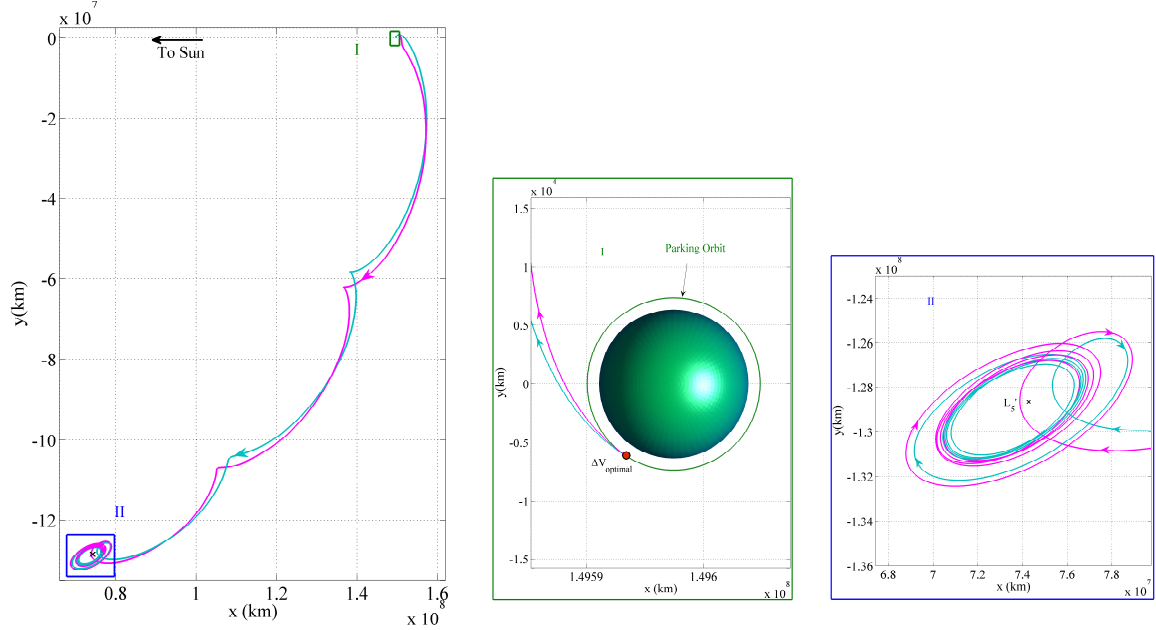
$$\text{where} \quad \vec{V}_1 = [V_{x_1} \ V_{y_1} \ V_{z_1}]^T = \vec{X}_1(\tau_{0_1})[4:6] \quad (22)$$

$$\vec{V}_c = [V_{x_c} \ V_{y_c} \ V_{z_c}]^T \quad (23)$$

$$\Delta \vec{V} = \vec{V}_1 - \vec{V}_c \quad (24)$$

From the definition, \vec{V}_1 is the velocity vector of the first patch point at initial time, τ_{01} . \vec{V}_c is the velocity vector at the departure location of the spacecraft from the Earth parking orbit. The equality constraints in Equation 21 are to maintain position and velocity continuity along each arc and the last entry in the constraint vector enforces departure from 1000 km parking orbit. The design variables comprises of three position components, three velocity components, two angles for each patch point, n , and $n - 1$ integration times between n patch points, thus, resulting in the design variable vector, \vec{X} of dimensions $(9n - 1) \times 1$.

The optimization problem is solved using Matlab's `fmincon` function that attempts to find a constrained minimum subject to nonlinear equalities or inequalities defined in a nonlinear constraint function. Thus, the problem is referred to as constrained nonlinear optimization. The process is started by providing the solar sail end-to-end trajectory designed in Section and illustrated in Figure 10(a) (light-blue) as an initial guess. Applying the described optimization scheme, the resulting transfer with local optimal departure maneuver, $\Delta V_{optimal}$ appears in Figure 13 along with the initial guess. The optimization process alters the solar sail



(a) Sail transfer trajectories with optimal (magenta) and non-optimal (light-blue) departure ΔV from Earth orbit to the vicinity of L_5 . (b) Departure from Earth parking orbit with $\Delta V_{optimal} = 3.0060$ km/s. (c) Arrival trajectories in the vicinity of displaced L_5' (black \times).

Figure 13: Sail trajectories for $\beta = 0.022$ with optimal (magenta) and non-optimal (light-blue) departure ΔV .

trajectory as depicted by magenta trajectory in Figure 13(a) and gives $\Delta V_{optimal}$ relative to the non-optimal case in light-blue. As expected with the optimization routine, the overall architecture remains similar to that of a good initial guess. Departure trajectories from 1000 km Earth parking orbit are illustrated in Figure 13(b). The blue trajectory depicts the sail-based departure from the parking orbit with non-optimal ΔV . The optimal departure maneuver, $\Delta V_{optimal}$ location is marked by the red dot along the parking orbit that delivers the spacecraft onto the magenta sail-based trajectory. The required change in velocity to deliver the spacecraft from the Earth parking orbit onto the sail-based transfer arc is $\Delta V_{optimal} = 3.0060$ km/s. In this scenario, the optimization scheme lowered the departure ΔV by 28.1 m/s. The arrival in the vicinity of the displaced Lagrange point, L_5' is illustrated in Figure 13(c) for the local optimal and non-optimal departures. As a result of the optimization process, the TOF for the local optimal case increased by ≈ 7 days.

As a part of testing and building on the strategy outlined for applying solar sails to the trajectory design process and optimizing the departure ΔV , additional values for β are tested as listed in Table 1. The values of β selected are based on current technology capabilities and are within the range of proposed short-term Geostorm and the Sunjammer missions.^{29,30} The first column identifies the case starting with the converged

Case	β	$ \Delta\psi $	TOF (years)	$\Delta V_{departure}$ (km/s)	$\Delta V_{arrival}$ (km/s)
No sail	–	–	2.88	3.041	559
Optimal 1	0.022	7.62°	2.94	3.006	0
Optimal 2	0.032	5.49°	2.90	2.994	0
Optimal 3	0.042	7.37°	2.90	2.988	0

Table 1. Departure ΔV optimization results for sail parameter, β , values compared to no sail case.

solution in classical CR3BP with no sail. Following the no sail case, three transfer trajectories with different values for sail parameter, β were converged by sail-based corrections scheme and supplied to the optimization routine as an initial guess. Column 3 gives the absolute value for the change in sail orientation angle, ψ for the optimized transfer trajectory. Column 4 is the total time of flight (TOF) for each case to reach the vicinity, marked by dotted-blue circle, of displaced L_5 . Note that the TOF for the no sail case is relatively lower than the three cases corrected and optimized with the solar sail. Column 5 gives the maneuver requirements in the form of $\Delta V_{departure}$ from the Earth parking orbit onto the transfer trajectory. As evident from column 6, no arrival ΔV is needed in the three sail based cases in contrary to the no sail case that requires a $\Delta V_{departure}$ equivalent to 559 m/s for the spacecraft to insert into an L_5 short period orbit. Thus, by leveraging SRP to maneuver the solar sail, the spacecraft demonstrate the capability to achieve the desired trajectory in the vicinity of displaced Lagrange points. Cost comparison is carried out with previous work in the literature. Lo, Llanos, and Hintz provided preliminary characterization for a typical L_5 mission and gave a case-by-case detailed table for overall performance.⁶ The results achieved in this work on solar sail transfer trajectory design are promising in comparison to the data provided by the authors. Comparing the case for final insertion into an orbit with approximate amplitude of 0.047 AU, the ΔV requirement ranges from 3.74 – 5.01 km/s for a departure from a 200 km parking orbit in the CR3BP. Whereas in the work presented here, implementing solar sail in the design scheme enabled harnessing the SRP to explore trajectory design options to Sun-Earth L_5 . Recall that the departure altitude for this investigation was maintained at an altitude of 1000 km, keeping in consideration the effectiveness of the solar sail and avoiding atmospheric drag. However, the transfer trajectories accomplished with the sail reflect the advantages of leveraging the SRP to maneuver the spacecraft. Thus, the overall propulsion requirements in the form of ΔV can potentially be lowered by incorporating solar sail dynamics in the trajectory design process to the vicinity of L_4 and L_5 .

CONCLUSIONS

To summarize, trajectory design options, incorporating solar sail dynamics, from the Earth parking orbit to the vicinity of triangular Lagrange points are explored. In particular, one transfer strategy is investigated in depth that utilizes the unstable manifold associated with an L_1 Lyapunov orbit to depart from the Earth parking orbit, arrive in the vicinity of the displaced Lagrange point, L_5 and maintain a trajectory close to the artificial libration point with the help of the solar sail. The sail angle in the form of $|\Delta\psi|$ in the inertial frame provided a promising results for reorientation of the sail that are within the technological capabilities of today. The optimization scheme further assisted in investigating the ΔV requirement to leave the Earth parking orbit. The trajectory analysis demonstrated that by incorporating solar sail in the dynamical model, solar radiation pressure can be leveraged to maneuver the sail-based spacecraft. Thus, solar sails provide transfers and trajectory design options to the vicinity of triangular Lagrange points enabling solar observations and exploration of potential Earth Trojans.

REFERENCES

- [1] M. Ozimek, D. Grebow, and K. Howell, “Design of solar sail trajectories with applications to lunar south pole coverage,” *Journal of guidance, control, and dynamics*, Vol. 32, No. 6, 2009, pp. 1884–1897.
- [2] G. G. Wawrzyniak and K. C. Howell, “Generating solar sail trajectories in the earth-moon system using augmented finite-difference methods,” *International Journal of Aerospace Engineering*, Vol. 2011, 2011.
- [3] N. Gopalswamy, J. Davila, O. S. Cyr, E. Sittler, F. Auchère, T. Duvall, J. Hoeksema, M. Maksimovic, R. MacDowall, A. Szabo, and M. Collier, “Earth-Affecting Solar Causes Observatory (EASCO): A potential International Living with a Star Mission from Sun–Earth L_5 ,” *Journal of Atmospheric and Solar-Terrestrial Physics*, Vol. 73, apr 2011, pp. 658–663, 10.1016/j.jastp.2011.01.013.

- [4] M. Connors, P. Wiegert, and C. Veillet, "Earth's Trojan asteroid," *Nature*, Vol. 475, jul 2011, pp. 481–483, 10.1038/nature10233.
- [5] A. A. Christou and D. J. Asher, "A long-lived horseshoe companion to the Earth," *Monthly Notices of the Royal Astronomical Society*, Vol. 414, apr 2011, pp. 2965–2969, 10.1111/j.1365-2966.2011.18595.x.
- [6] M. W. Lo, P. J. Llanos, and G. R. Hintz, "An L₅ Mission to Observe The Sun and Space Weather, Part I," *20th AAS/AIAA Space Flight Mechanics Meeting*, San Diego, California, February 2010.
- [7] P. Llanos, J. Miller, and G. Hintz, "Navigation Analysis for an L₅ Mission in the Sun-Earth System," *AIAA/AAS Astrodynastic Specialist Conference*, Vol. 142, Girdwood, Alaska, AAS 10-121, aug 2011.
- [8] N. Gopalswamy and EASCO Team, "Earth-Affecting Solar Causes Observatory (EASCO): Results of the Mission Concept Study," *AAS/Solar Physics Division Abstracts #42*, May 2011, p. 1518.
- [9] P. Llanos, J. Miller, and G. Hintz, "Mission and Navigation Design of Integrated Trajectories to L₄, 5 in the Sun-Earth System," *AIAA/AAS Astrodynastic Specialist Conference*, American Institute of Aeronautics and Astronautics (AIAA), aug 2012, 10.2514/6.2012-4668.
- [10] R. Dvorak, C. Lhotka, and L. Zhou, "The orbit of 2010 TK7: possible regions of stability for other Earth Trojan asteroids," *Astronomy & Astrophysics*, Vol. 541, 2012, p. A127.
- [11] P. J. Llanos, G. R. Hintz, M. W. Lo, and J. K. Miller, "Powered Heteroclinic and Homoclinic Connections between the Sun-Earth Triangular Points and Quasi-Satellite Orbits for Solar Observations," *AAS/AIAA Astrodynamics Specialist Conference*, AAS, 2013, pp. 13–786.
- [12] K. John, L. Graham, and P. Abell, "Investigating Trojan Asteroids at the L₄/L₅ Sun-Earth Lagrange Points," *Lunar and Planetary Science Conference*, Vol. 46, 2015, p. 2845.
- [13] C. McInnes, "Solar sailing. Technology, dynamics and mission applications., by McInnes, CR. Springer, London (UK), 1999, XXIX+ 296 p., ISBN 1-85233-102-X, Vol. 1, 1999.
- [14] O. Mori, Y. Tsuda, H. Sawada, R. Funase, T. Saiki, K. Yonekura, H. Hoshino, H. Minamino, T. Endo, J. Kawaguchi, *et al.*, "World's First Demonstration of Solar Power Sailing by IKAROS," *The Second International Symposium on Solar Sailing*, 2010.
- [15] J. Davis, "LightSail Test Mission Declared Success; First Image Complete," <http://sail.planetary.org/>, 2015.
- [16] C. Biddy, "Presentation: LightSail-1 Solar Sail Design and Qualification (via <http://www.planetary.org/blogs/bruce-betts/20120531-LightSail-Biddy-Presentation.html>)," *41st Aerospace Mechanisms Symposium*, Pasadena, CA, USA, 2012.
- [17] H. Baoyin and C. R. McInnes, "Solar sail halo orbits at the Sun–Earth artificial L₁ point," *Celestial Mechanics and Dynamical Astronomy*, Vol. 94, No. 2, 2006, pp. 155–171.
- [18] K. C. Howell, "Three-dimensional, periodic, 'halo orbits,'" *Celestial Mechanics*, Vol. 32, No. 1, 1984, pp. 53–71.
- [19] C. R. McInnes, A. J. McDonald, J. F. Simmons, and E. W. MacDonald, "Solar sail parking in restricted three-body systems," *Journal of Guidance, Control, and Dynamics*, Vol. 17, No. 2, 1994, pp. 399–406.
- [20] R. Sood, "Solar sail applications for mission design in sun-planet systems from the perspective of the circular restricted three-body problem," Master's thesis, Purdue University, West Lafayette, IN, Dec. 2012. ProQuest: AAI1535164.
- [21] T. J. Waters and C. R. McInnes, "Periodic orbits above the ecliptic in the solar-sail restricted three-body problem," *Journal of Guidance, Control, and Dynamics*, Vol. 30, No. 3, 2007, pp. 687–693.
- [22] J. Simo and C. McInnes, "Solar sail trajectories at the Earth-Moon Lagrange points," *59th International Astronautical Congress (IAC'08)*, 2008.
- [23] J. Heiligers, S. Hiddink, R. Noomen, and C. R. McInnes, "Solar sail Lyapunov and Halo orbits in the Earth–Moon three-body problem," *Acta Astronautica*, Vol. 116, 2015, pp. 25–35.
- [24] G. Gómez, J. Llibre, R. Martínez, and C. Simó, *Dynamics and Mission Design Near Libration Points, Vol. I Fundamental: The Case of Collinear Libration Points*. Singapore: World Scientific, 2001.
- [25] V. Szebehely, *Theory of Orbits: The Restricted Problem of Three Bodies*. New York: Academic Press, 1967.
- [26] B. T. Barden and K. C. Howell, "Fundamental Motions Near Collinear Libration Points and Their Transitions," *The Journal of the Astronautical Sciences*, Vol. 46, No. 4, 1998, pp. 361–378.
- [27] J. L. Wright and A. Kantrowitz, "Space Sailing," *Phys. Today*, Vol. 45, No. 12, 1992, p. 85, 10.1063/1.2809919.
- [28] Y. Tsuda, O. Mori, R. Funase, H. Sawada, T. Yamamoto, T. Saiki, T. Endo, K. Yonekura, H. Hoshino, and J. Kawaguchi, "Achievement of IKAROS – Japanese deep space solar sail demonstration mission," *Acta Astronautica*, Vol. 82, No. 2, 2013, pp. 183–188.
- [29] M. Macdonald and C. McInnes, "Solar sail science mission applications and advancement," *Advances in Space Research*, Vol. 48, No. 11, 2011, pp. 1702–1716.
- [30] J. Heiligers and C. McInnes, "Novel solar sail mission concepts for space weather forecasting," *24th AAS/AIAA Space Flight Mechanics Meeting 2014*, 2014.
- [31] B. Wie, "Solar Sail Attitude Control and Dynamics, Part Two," *Journal of Guidance, Control, and Dynamics*, Vol. 27, No. 4, 2004, pp. 536–544.